Polarization Mode Dispersion Detected by Arrival Time Measurement of Polarization-Scrambled Light

R. Noé, *Member, IEEE*, D. Sandel, V. Mirvoda, F. Wüst, and S. Hinz

***Abstract*—Polarization mode dispersion (PMD) limits optical fiber capacity. PMD compensators usually minimize the associated eye closure. This measure scales with the square of the differential group delay (DGD) and makes it difficult to detect low DGDs. However, light with a low-speed polarization modulation suffers arrival time variations, in the presence of PMD, that are proportional to the DGD. These are detected by integrating the voltage-controlled oscillator (VCO) input signal of the clock recovery phase-locked loop (PLL). This novel method has been demonstrated for 40 Gb/s nonreturn-to-zero (NRZ) and for 2 × 40 Gb/s return-to-zero (RZ) polarization division multiplex transmission. PMD detection sensitivities range between 2 ps and 84 fs.**

***Index Terms*—Optical fiber communication, polarization, polarization mode dispersion (PMD).**

I. Introduction

POLARIZATION mode dispersion (PMD) compensators need fast and accurate PMD detection at low cost. To our knowledge, all published purely electrical methods (e.g., [1]–[3]) detect quantities comparable to the eye opening. In the limit of a first-order differential group delay (DGD) τ that is small compared to the bit duration, the error signals are proportional to τ^2 and, hence, extremely weak. The same holds also for degree-of-polarization measurements [4], unless the pulse edges are shorter than τ. Here, we measure arrival time variations of polarization-scrambled light by integrating the voltage-controlled oscillator (VCO) input signal of the clock recovery phase-locked loop (PLL) in the receiver. This generates error signals proportional to τ, or parts thereof, and allows the detection of PMD at or below the eye pattern visibility limit. Section II describes methods and experiments for standard single-polarization transmission. Current development of high-end systems appears to be moving toward polarization division multiplex (PolDM) [5], [6] and return-to-zero (RZ) transmission. Section III shows theoretically and experimentally how the method is implemented with minimum cost and superior performance in RZ PolDM systems.

In an environment with PMD compensator, first-order PMD of transmission fiber and compensator add vectorially. The length of the sum vector (or of its detrimental components) is the residual first-order DGD (or its detrimental part). Minimizing this quantity, which is measured in the setups described hereafter, will provide optimum PMD compensation. The optical PMD compensator itself may be any nondichroic type, such as that described in [3], [7].

The motivation for this work is mainly to generate high-quality error signals for control of optical PMD compensators, although the method could also be used for online instrumentation purposes.

II. Standard Single-Polarization Transmission

A. Theory

The electric field vector envelope of a horizontally polarized signal is

$$\mathbf{E}_0(t) = \begin{bmatrix} b(t) \\ 0 \end{bmatrix} \tag{1}$$

where $b(t) \in \{0, 1\}$ is a time-dependent (t) binary bit pattern. Consider a Jones matrix $\mathbf{J}(t)$ that consists of bandpass impulse responses, which allows the calculation of the received electric field vector envelope $\mathbf{E}(t)$ by convolution

$$\mathbf{E}(t) = \mathbf{J}(t) * \mathbf{E}_0(t). \tag{2}$$

For a medium with pure first-order PMD [8] and a corresponding differential group delay (DGD) τ, we can write without loss of generality

$$\mathbf{J}(t) = \mathbf{RQ}\begin{bmatrix} \delta(t+\tau/2) & 0 \\ 0 & \delta(t-\tau/2) \end{bmatrix}\mathbf{Q}^+. \tag{3}$$

$\mathbf{Q}$, $\mathbf{R}$ are constant unimodular matrices. It is useful to set

$$\mathbf{Q} = \frac{1}{\sqrt{2(1+\Omega_{1n})}}\begin{bmatrix} 1+\Omega_{1n} & -\Omega_{2n} - j\Omega_{3n} \\ \Omega_{2n} - j\Omega_{3n} & 1+\Omega_{1n} \end{bmatrix} \quad (\Omega_{1n}^2 + \Omega_{2n}^2 + \Omega_{3n}^2 = 1) \tag{4}$$

where $\boldsymbol{\Omega}_n = [\Omega_{1n}\ \Omega_{2n}\ \Omega_{3n}]^T$ is the normalized Stokes vector of the (input-referred) fast principal state of polarization (PSP). The PMD vector is $\boldsymbol{\Omega} = [\Omega_1\ \Omega_2\ \Omega_3]^T = \boldsymbol{\Omega}_n\tau$.

Using $|b(t)|^2 = b(t)$, the normalized photocurrent in the receiver is calculated as

$$I(t) = |\mathbf{E}(t)|^2 = \tfrac{1}{2}\left((1+\Omega_{1n})b_+ + (1-\Omega_{1n})b_-\right) \tag{5}$$

where $b_\pm$ stands for $b(t \pm \tau/2)$. The arrival time of the signal is most easily determined if one assumes a single rectangular pulse

$$b(t) = \begin{cases} 1, & |t| < t_p/2 \\ 0, & \text{else} \end{cases}$$

Manuscript received June 13, 2001; revised October 16, 2001. This work was supported in part by Siemens ICN and Deutsche Forschungsgemeinschaft.

R. Noé, D. Sandel, V. Mirvoda, and F. Wüst are with the University of Paderborn, Optical Communications and High-Frequency Engineering, Paderborn 33098, Germany.

S. Hinz was with the University of Paderborn, Optical Communications and High-Frequency Engineering, Paderborn 33098, Germany. He is now with Siemens KN, München 81359, Germany.

Publisher Item Identifier S 0733-8724(02)00498-X.

0733–8724/02$17.00 © 2002 IEEE

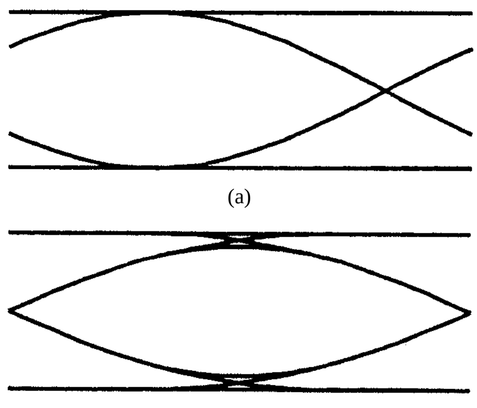

Fig. 1. Standard NRZ transmission in the presence of 1st-order PMD with $\tau/T = 3/8$ for (a) fast PSP transmission and (b) fast–slow PSP mixture.

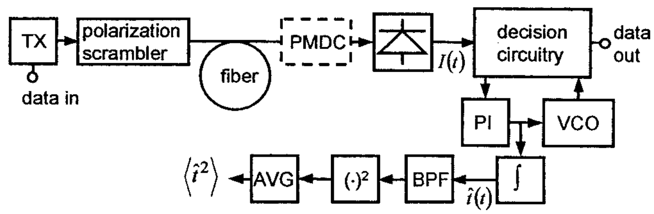

Fig. 2. Arrival time detection for standard single-polarization transmission.

centered at the time origin. For nonreturn-to-zero (NRZ) pulses, t_p equals the bit duration T; for RZ pulses, $t_p < T$ holds. The arrival time

$$\hat{t} = \frac{\int tI(t)\,dt}{\int I(t)\,dt} \tag{6}$$

defined as the gravity center of the received pulse is

$$\hat{t} = -\Omega_{1n}\tau/2 = -\Omega_1/2. \tag{7}$$

Consider NRZ photocurrent pulses that pass through an electrical baseband filter. It has a cosine-shaped impulse response $\cos(\pi t/T)$ ($|t| < T/2$) that lasts one bit duration. For $\Omega_{1n} = 0$, the relative eye opening is $\cos(\pi\tau/(2T))$. For small τ, the eye closure scales with $(\tau/T)^2$ [Fig. 1(b)]. That effect is much more difficult to detect than arrival time variations occurring between $\Omega_{1n} = 1$ [Fig. 1(a)] and $\Omega_{1n} = -1$ [not shown; mirror-symmetric to Fig. 1(a)], which scale linearly with τ.

Arrival time differences can be generated if the power splitting ratio into the PSPs of the transmission fiber is modulated by a polarization scrambler that is placed between transmitter TX and fiber (Fig. 2). If one considers scrambler and fiber to be one unit, then its PSPs are modulated, so this calculation is applicable. Ideal polarization scrambling is not essential here, so accuracy requirements are moderate. The cost of the scrambler becomes negligible if it is shared among many WDM channels. These have fixed but unknown polarizations at the scrambler input. A scrambler that operates independently of its input polarization is, therefore, needed. It can be constructed from $\lambda/4$ and $\lambda/2$ plates rotating at different speeds, or the electro- (or acoustooptical) analogons thereof [9]–[11]. Concatenation [10] can overcome even severe shortcomings of individual nonideal scramblers. An ideal scrambler will make mean and root mean square (rms) value of each normalized Stokes parameter at its output equal to 0 and $1/\sqrt{3}$, respectively, and the normalized Stokes parameters will be uncorrelated. In Fig. 1, the arrival time $\hat{t}(t)$ is, therefore, modulated by the scrambler, and its variance is $\langle\hat{t}^2\rangle = \tau^2/12$.

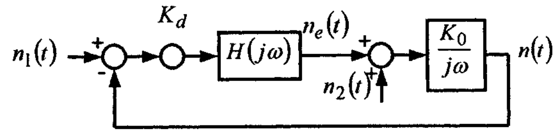

Fig. 3. Clock recovery PLL.

It has been verified numerically that this arrival time modulation also exists and is usable if the signal carries additional distortions due to higher-order PMD.

The arrival time of slopes and pulses is reflected by the recovered clock phase, provided that the clock PLL is faster than the modulation impressed by the scrambler. The clock is generated by a voltage-controlled oscillator VCO. Clock time errors may, for example, be determined in a decision circuitry according to [12]. The clock time error is the input signal of a proportional-integral controller polarization index (PI), which, in turn, controls the VCO. Its frequency control input contains a signal that is proportional to the temporal derivative $d\hat{t}(t)/dt$ of the arrival time. An integrator or a lowpass filter with a very low cutoff frequency yields $\hat{t}(t)$. Behind a bandpass filter (BPF) for noise reduction, the variance $\langle\hat{t}^2\rangle$ is determined by a squarer with subsequent averaging circuit AVG or integrator. It may serve to control a PMD compensator.

We assess now the achievable PMD detection sensitivity by calculating the DGD noise variance. With respect to Fig. 3, $n_1(t)$, $N_1(j\omega)$ are the received clock phase (rad) and its spectrum, respectively. These contain also white noise with a constant two-sided spectral density L_1. Quantities $n(t)$, $N(j\omega)$ are the VCO output clock phase (rad) and its spectrum, respectively, K_d is the phase detector slope (e.g., V/rad), and $H(j\omega)$ is the proportional-integral controller transfer function. The controller output signal to be measured (e.g., V) and its spectrum are $n_e(t)$, $N_e(j\omega)$, respectively. Inside the VCO, white Gaussian frequency noise $n_2(t)$ and its spectrum $N_2(j\omega)$ are added. These are expressed here in the same units as the VCO controller output signal (e.g., V). The spectrum has a constant two-sided spectral density L_2. The VCO slope (e.g., Hz/V) is K_o.

The clock recovery PLL is governed by

$$\begin{aligned}(N_1(j\omega) - N(j\omega))\,K_d H(j\omega) &= N_e(j\omega)\\ (N_2(j\omega) + N_e(j\omega))\,\frac{K_o}{j\omega} &= N(j\omega).\end{aligned} \tag{8}$$

Usually, a proportional-integral controller is chosen

$$H(j\omega) = \frac{\tau_2}{\tau_1} + \frac{1}{j\omega\tau_1}. \tag{9}$$

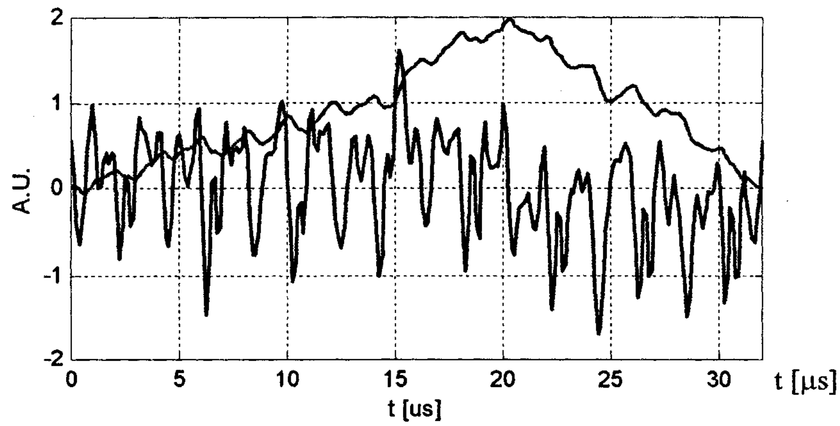

Fig. 4. VCO input signal at 0.77 ps of DGD (periodic curve) and inferred arrival time (top smooth curve).

This results in transfer functions

$$\frac{N}{N_1} = -\frac{N_e}{N_2} = \frac{2jx\xi + 1}{-x^2 + j2\xi x + 1}$$
$$\frac{N}{N_2} = \frac{K_o}{\omega_r}\,\frac{jx}{-x^2 + j2\xi x + 1}$$

with

$$\omega_r = \sqrt{\frac{K_d K_o}{\tau_1}} \qquad \xi = \frac{\tau_2}{2}\,\omega_r \qquad x = \frac{\omega}{\omega_r}. \tag{10}$$

The clock phase noise caused by the received clock phase has the variance

$$\sigma_{n,n_1}^2 = \frac{1}{2\pi}\int_{-\infty}^{\infty}\left|\frac{N}{N_1}\right|^2 L_1 d\omega = \frac{\omega_r L_1}{4\xi}\,(4\xi^2+1). \tag{11}$$

The power spectral density $L_1 K_d^2$ of the white spectrum of the received phase noise can be measured after the phase detector to determine L_1, using the transmitter clock signal and no PLL. The variance of the clock phase noise caused by white Gaussian frequency noise is

$$\sigma_{n,n_2}^2 = \frac{1}{2\pi}\int_{-\infty}^{\infty}\left|\frac{N}{N_2}\right|^2 L_2 d\omega = \frac{K_0^2 L_2}{4\xi\omega_r}. \tag{12}$$

Here, $L_2 = 2\pi\Delta f K_0^{-2}$ if the clock signal has a Lorentzian line with a width Δf. The total clock phase variance is

$$\sigma_n^2 = \sigma_{n,n_1}^2 + \sigma_{n,n_2}^2. \tag{13}$$

We introduce a normalization constant $A = \sigma_{n,n_1}^2/\sigma_n^2$ $(0 < A < 1)$. Assume that the integrator also contains an equalizing filter with a transfer function N_1/N in the frequency range $\omega_1 < \omega < \omega_2$. In reality, this filter will normally not be needed because $N_1/N \approx 1$ for $|\omega| \ll \omega_r$, i.e., for a fast clock PLL. The bandpass filter passes $\omega_1 < \omega < \omega_2$. The resulting DGD noise variance is

$$\begin{aligned}\langle \hat{t}_n^2\rangle &= \left(\frac{T}{2\pi}\right)^2 2\,\frac{1}{2\pi}\int_{\omega_1}^{\omega_2}\left(\left|\frac{N}{N_1}\right|^2 L_1 + \left|\frac{N}{N_2}\right|^2 L_2\right)\left|\frac{N_1}{N}\right|^2 d\omega \\ &= \left(\frac{T}{2\pi}\right)^2 \sigma_n^2\,\frac{4\xi}{\pi}\int_{\omega_1/\omega_r}^{\omega_2/\omega_r}\frac{1}{4\xi^2x^2+1} \\ &\quad\cdot\left(A\frac{1-x^2}{4\xi^2+1}+x^2\right)dx. \end{aligned} \tag{14}$$

The quotient $\langle \hat{t}^2\rangle/\langle \hat{t}_n^2\rangle$ is the signal-to-noise ratio (SNR) for DGD measurement.

B. Experiment

This technique was implemented in a 40-Gb/s NRZ transmission system (Fig. 2). The polarization scrambler consisted of an electrooptical rotating $\lambda/4$ wave plate and a counter-rotating $\lambda/2$ plate, both driven at 250 kHz. Integration and rms detection were implemented digitally. Measurement intervals were 4 μs or one period of the polarization modulation. Erbium-doped fiber amplifiers (EDFAs) are not shown for simplicity. Fig. 4 shows exemplary signals for a test module (PMD) with 0.77 ps of DGD. These changed by several decibels as a function of polarization settings in front of and behind the scrambler. Regarding PMD compensation, this is uncritical as long as the PMD equalizer is able to eliminate essentially all PMD. As mentioned in the introduction, any usual PMD compensator can be used for this purpose.

Only the fast modulation of the inferred arrival time is evaluated; its slow ascent and descent is due to VCO phase noise. The recovered clock shows sidebands at multiples of the polarization modulation frequency, and so does the prescaled (1 : 2) clock spectrum shown in Fig. 5. Fig. 6 shows eye patterns obtained from an additional 50-GHz monitor photodiode. Because it was triggered from the TX, there is horizontal eye closure due to PMD, and maybe also some due to the interplay of TX clock linewidth and propagation delay. Between 0 and 2 ps of DGD, there is little, if any, difference. At 5.5 ps of DGD, essentially horizontal eye closure is visible, due to arrival time modulation, but no vertical eye closure. This is where other methods to detect PMD often fail while arrival time detection is still at ease. At 19 ps of DGD, the eye is almost completely closed.

$\Delta\hat{t}_{\mathrm{rms}}$ values measured with the least favorable scrambler input polarization are plotted in Fig. 7. The value for 19 ps and the offset at 0 ps (back-to-back including scrambler) allowed a theoretical curve fit, assuming there is a constant background power. For each DGD point, n independent data samples d_i $(i = 1\cdots n)$ were taken, and the standard deviation within this sample set was calculated by

$$\sigma = \sqrt{\frac{1}{n-1}\sum_i\left(d_i - \frac{1}{n}\sum_j d_j\right)^2}.$$

Nonoverlapping ± 1-σ error intervals (also shown) between data at 0 ps and 2 ps indicated a detection limit of 2ps. The setup was

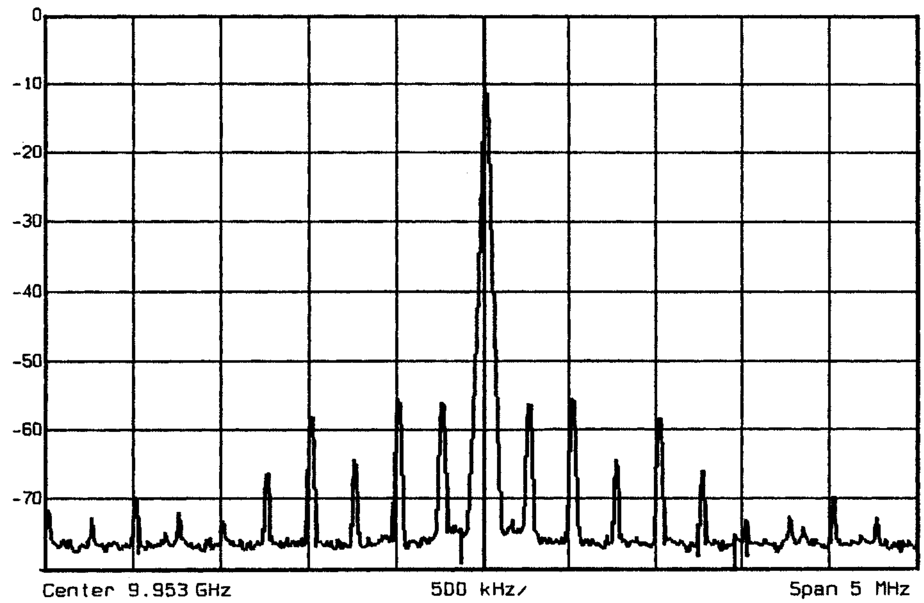

Fig. 5. Spectrum of prescaled (10 GHz) recovered clock signal in the presence of 0.77 ps of DGD.

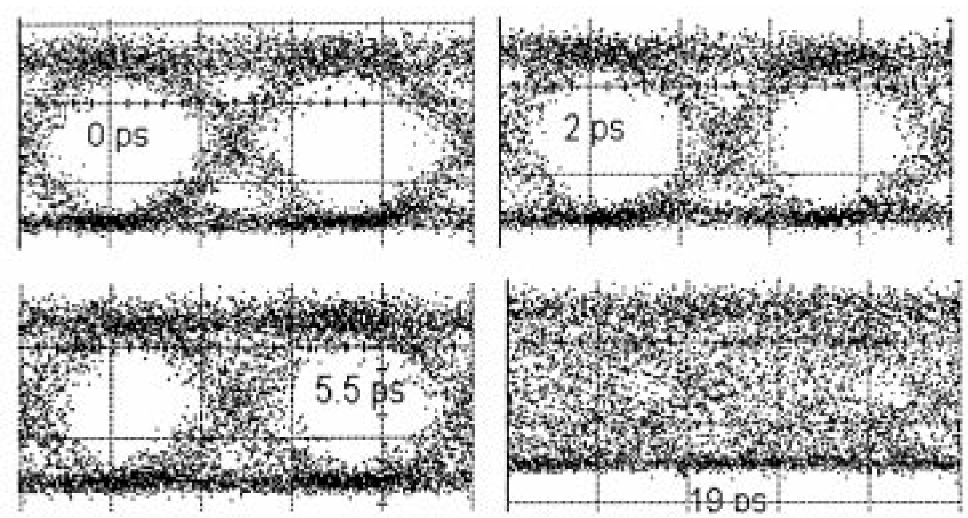

Fig. 6. 40-Gb/s eye patterns at 0, 2, 5.5, and 19 ps of DGD.

not optimized, and it should not be difficult to reach a higher detection efficiency.

III. RZ Polarization Division Multiplex Transmission

A. Theory

PolDM transmission of two data signals on one optical carrier is attractive to double fiber capacity [5]. RZ PolDM transmission has been demonstrated, and interchannel interference was detected to correct polarization mismatch at the receiver [6]. We assume the two binary bit patterns $b_k(t) \in \{0, 1\}$ ($k = 1, 2$) to be bit synchronous, not bit interleaved. The phase difference between the two data channels is φ. The transmitted electric field vector envelope is

$$\mathbf{E}_0(t) = \begin{bmatrix} b_1(t) \\ e^{-j\varphi} b_2(t) \end{bmatrix}. \tag{15}$$

For perfect polarization control

$$\mathbf{R} = \begin{bmatrix} e^{j\xi/2} & 0 \\ 0 & e^{-j\xi/2} \end{bmatrix} \tag{16}$$

must hold in (3). The normalized photocurrents $I_k(t) = |E_k(t)|^2$ ($k = 1, 2$) are

$$\begin{aligned} I_1(t) = &\tfrac{1}{4}\left((1+\Omega_{1n})b_{1+} + (1-\Omega_{1n})b_{1-}\right)^2 \\ &+ \tfrac{1}{4}(\Omega_{2n}^2 + \Omega_{3n}^2)(b_{2+} - b_{2-})^2 \\ &+ \tfrac{1}{2}\sqrt{\Omega_{2n}^2 + \Omega_{3n}^2}\cos\left(\varphi - \arg(\Omega_{2n} + j\Omega_{3n})\right) \\ &\cdot \left((1+\Omega_{1n})b_{1+} + (1-\Omega_{1n})b_{1-}\right)(b_{2+} - b_{2-}) \\ I_2(t) = &\tfrac{1}{4}\,(\Omega_{2n}^2 + \Omega_{3n}^2)(b_{1+} - b_{1-})^2 \\ &+ \tfrac{1}{4}\left((1-\Omega_{1n})b_{2+} + (1+\Omega_{1n})b_{2-}\right)^2 \\ &+ \tfrac{1}{2}\sqrt{\Omega_{2n}^2 + \Omega_{3n}^2}\cos\left(\varphi - \arg(\Omega_{2n} + j\Omega_{3n})\right) \\ &\cdot \left((1-\Omega_{1n})b_{2+} + (1+\Omega_{1n})b_{2-}\right)(b_{1+} - b_{1-}). \end{aligned} \tag{17}$$

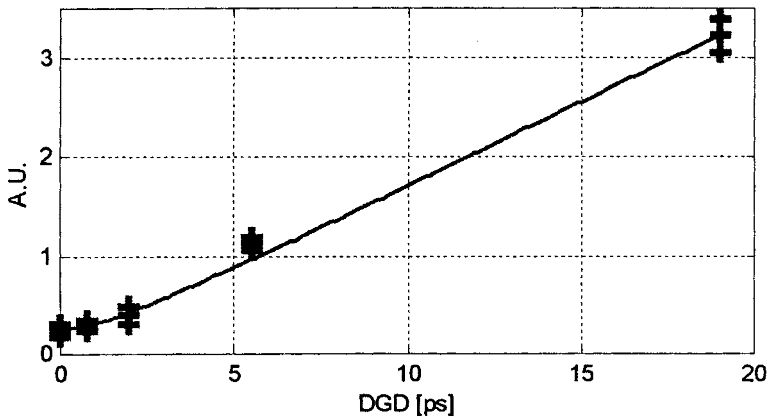

Fig. 7. rms arrival time variation $\Delta\hat{t}_{\rm rms}$ versus DGD (ps).

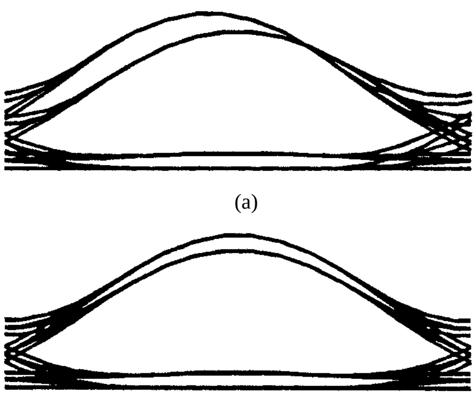

(a)

(b)

Fig. 8. PolDM RZ in the presence of first-order PMD with $\tau/T = 1/8, \Omega_1 = 0$ for maximum (a) $\Delta\hat{t} = \sqrt{\Omega_2^2 + \Omega_3^2}$ and (b) $\Delta\hat{t} = 0$.

Here, E_k are the components of $\mathbf{E}$, and $b_{k\pm}$ stands for $b_k(t \pm \tau/2)$. For simplicity, let us take the limit $\tau \ll t_p$. For

$$b_1(t) = \begin{cases} 1, & |t| < t_p/2 \\ 0, & \text{else} \end{cases}$$

and $b_2(t) = 0$, application of (6) yields a pulse arrival time $\hat{t}_1 = -\Omega_1/2$ in receiver 1. If both data channels carry pulses, $b_2(t) = b_1(t)$, the pulse in receiver 1 arrives at $\hat{t}_1 = -\Omega_1/2 - \sqrt{\Omega_2^2 + \Omega_3^2}/2 \cdot \cos(\varphi - \arg(\Omega_{2n} + j\Omega_{3n}))$. These are the only cases that can occur for RZ signals. The average over the two equiprobable cases is the mean pulse arrival time of receiver 1

$$\langle \hat{t}_1 \rangle = -\Omega_1/2 - \Delta\hat{t}/4$$

with

$$\Delta\hat{t} = \sqrt{\Omega_2^2 + \Omega_3^2} \cos\left(\varphi - \arg(\Omega_{2n} + j\Omega_{3n})\right), \quad \tau \ll t_p. \tag{18}$$

Fig. 8 shows eye diagrams for $\cos(\varphi - \arg(\Omega_{2n} + j\Omega_{3n}))$ equal to 1 [Fig. 8(a)] or 0 [Fig. 8(b)]. RZ pulse width is $T/2$. A similar calculation yields the mean pulse arrival time $\langle \hat{t}_2 \rangle = \Omega_1/2 - \Delta\hat{t}/4$ for receiver 2. Fig. 9 shows a setup suitable for exploiting these findings.

The signal from a single transmitter laser is split 1 : 1 into two arms, one of which suffers a delay $\tilde{\tau}$. Each branch signal is intensity modulated by one RZ data signal. Usually, this would be done by a common RZ pulse modulator (RZ MOD) and one NRZ modulator (MOD) in each of the branches. Signals are recombined with orthogonal polarizations in a polarization beamsplitter (PBS). A sinusoidal frequency modulation (FM) with frequency F and a peak-to-peak optical frequency deviation $\Delta f_{\rm pp}$ is applied to the transmitter laser and results in a differential (interchannel) phase modulation. It has a Bessel spectrum with modulation index $\eta = \pi \Delta f_{\rm pp} \tilde{\tau} \operatorname{sinc}(\pi F \tilde{\tau})$. The phase difference is $\varphi = \overline{\varphi} + \eta \sin 2\pi F t$. Its mean value $\overline{\varphi}$ fluctuates with temperature. Another PBS demultiplexes the signals in the receiver. A signal processor (DSP) monitors detected interchannel interference terms and minimizes them by appropriate setting of a polarization controller (PC), as detailed in [6]. Observed clock time errors are added to form the input signal of the PI controller of the clock signal PLL. If, like in [6], the powers of at least one even and one odd Bessel line of the arrival time spectrum are detected and added, the quantity $\sqrt{\Omega_2^2 + \Omega_3^2}$ can be determined from $\Delta\hat{t}$. It can be minimized by suitable control of a PMD compensator. The difference of the two observed clock time errors is also determined. Without further control, it would be Ω_1. However, it is preferable to feed it to an integrator that drives a differential clock phase shifter DPS. Thus, the clock time difference is adjusted electronically to its optimum value Ω_1, and the clock time error difference vanishes. If the DPS operates linearly, its input signal is proportional to Ω_1. The DGD τ can also be determined from Ω_1 and $\sqrt{\Omega_2^2 + \Omega_3^2}$. If a clock phase shifter is undesirable, Ω_1 may be minimized by additional control of a PMD compensator.

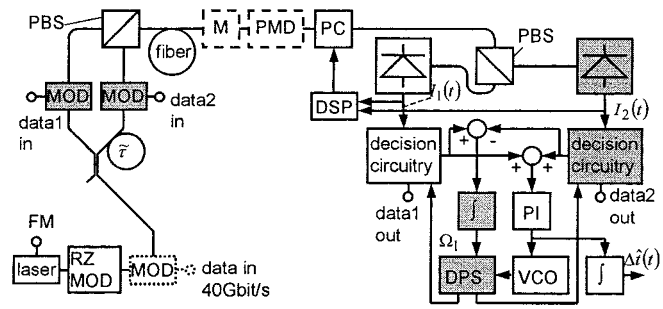

Fig. 9. Arrival time detection for RZ PolDM transmission.

For carrier-suppressed RZ pulses where both PolDM signals change electric field polarities simultaneously between subse-

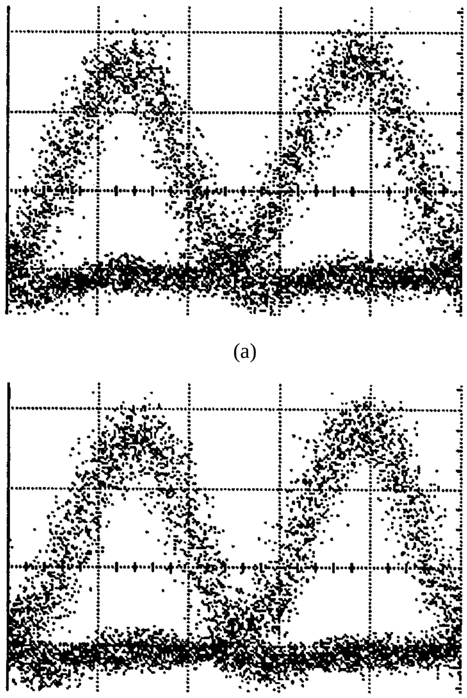

Fig. 10. RZ PolDM eye patterns at (a) 0 ps and (b) 2 ps of DGD, worst case.

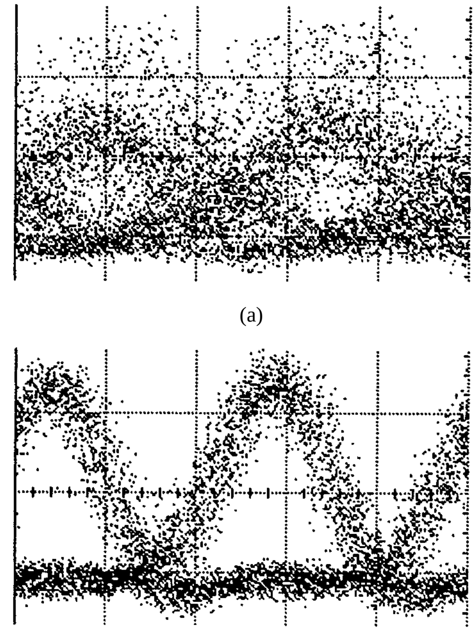

Fig. 11. RZ PolDM eye patterns at 10 ps of DGD, (a) worst case and (b) best case.

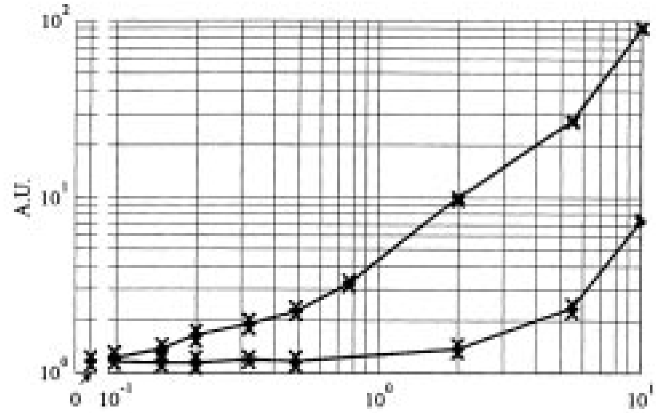

Fig. 12. $\Delta\hat{t}_{\mathrm{rms}}$ versus DGD (ps) measured in 4.8 μs. Zero DGD point is separated from logarithmic axis.

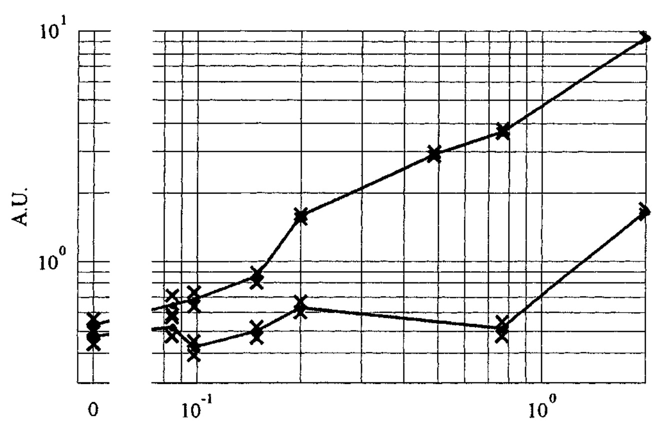

Fig. 13. $\Delta\hat{t}_{\mathrm{rms}}$ versus DGD (ps) measured in 38.4 μs. Zero DGD point is separated from logarithmic axis.

quent pulses, the sign of the interference signal will not change from bit to bit. As a result, the scheme is also applicable for carrier-suppressed RZ.

B. Experiment

Clock recovery was improved with respect to the previous experiment. A 2 $\times$ 40-Gb/s RZ PolDM transmission system was set up. A 417-kHz FM was applied to the TX laser to generate interchannel phase modulation with an index $\eta = 4.2$. A Mach–Zehnder modulator (RZ MOD) driven at 20 GHz generated a 40-GHz RZ pulse stream. For simplicity, a common data modulator (dotted MOD) was placed in front of the polarization multiplexer and all shaded components were left out. In the receiver, an x-cut z-propagation $LiNbO_3$ device served as a PC [13]. A linear combination of Bessel lines 2, 3, and 4 in the photocurrent was detected and minimized by DSP–PC. Similar processing of $\Delta\hat{t}(t)$ allowed the determination of the rms value $\Delta\hat{t}_{\mathrm{rms}}$ of $\Delta\hat{t}$ simultaneously. The VCO was connected directly to the decision circuitry without DPS. Eye patterns in the 50-GHz monitor receiver are shown in Figs. 10 and 11. For each DGD, the polarizations at the PMD module input were adjusted by a manual polarization transformer (M) for maximum $\Delta\hat{t}_{\mathrm{rms}}$ ($\Omega_1 = 0, \sqrt{\Omega_2^2+\Omega_3^2} = \max$) as the worst case [Figs. 10 (b) and 11(a), and top traces in Figs. 12 and 13], and for most DGDs also at minimum $\Delta\hat{t}_{\mathrm{rms}}$ ($|\Omega_1| = \max, \sqrt{\Omega_2^2+\Omega_3^2} = 0$) as the best case [Fig. 11(b) and bottom traces in Figs. 12 and 13]. Note that for 2 ps, the worst case eye pattern is not or hardly distinguishable from the 0-ps case (Fig. 10). The best case data should, theoretically, be constant for all DGDs. Upward bending of these curves for high DGDs is attributed to the difficulty of aligning the PSPs of the PMD device along the two transmitted polarizations. Worst case data should, theoretically, form a straight line with a slope of 1, but the slopes in Figs. 12 and 13 look more curved than that in Fig. 7. At low DGDs, this is due to the random background noise and the logarithmic scale. There could also be an upward bending at the highest measured DGD value of 10 ps, which is not believed to be critical. Other deviations from the linear correspondence may be due to the difficulty of setting $\sqrt{\Omega_2^2 + \Omega_3^2} = \max$ by hand.

The sensitivity limit, again defined by nonoverlapping $\pm 1 - \sigma$ error intervals (x symbols), was 150 fs (Fig. 12) and 84 fs (Fig. 13) for 4.8-μs- and 38.4-μs-long measurement intervals, respectively. Due to the high sensitivity, details at low DGDs are hard to be seen in these plots, but were accurately measured. The latter DGD is $6.5 \cdot 10^{-3}$ times the impulse duration ($\sim$13 ps) and belongs to a 42-mm-long piece of polarization-maintaining fiber (PMF) with less than 17 beat lengths. Such sensitive measurements normally require a radiofrequency (RF) network analyzer or an interferometric setup.

A natural question was whether we had, indeed, measured PMD or some other unwanted effect instead. In order to rule out such an error, the received power was halved, which influenced measured data either insignificantly or not at all. In another test, a 185-mm-long straight piece of polarizing fiber was inserted as a device under test. It had a polarization-dependent loss (PDL) of 0.08 dB, and our measurements at maximum $\Delta \hat{t}_{\mathrm{rms}}$ indicated a DGD of $\sim$750 fs. When it was bent, the PDL between its PSPs increased to 3.5 dB, and its DGD seemed to increase to 800 fs even though, in reality, it probably stayed constant. However, the small percentage of perceived DGD increase in spite of the large PDL change shows that PDL can have played only a minor role, and we have, in fact, measured DGDs. The standard deviations in Figs. 12 and 13 are small even for large DGDs, which gives additional credibility to the results.

IV. Conclusion

Arrival time detection of PSPs subject to PMD using the VCO input signal of the clock recovery yields a linear measure of the DGD. Experiments have been carried out for 40-Gb/s NRZ standard transmission and 2 $\times$ 40-Gb/s RZ polarization division multiplex transmission, with resulting PMD detection limits of 2 ps and 150 fs ... 84 fs, respectively. Both in absolute terms and normalized with respect to the impulse width, no better online PMD detection results have been reported, to our knowledge. Measurement speed is amply sufficient. No extra high-frequency electronics, nor any extra optics in each WDM channel, are required, other than for competing approaches. The discussed schemes should allow the realization of high-quality optical PMD compensators.

References

[1] T. Takahashi *et al.*, "Automatic compensation technique for timewise fluctuating polarization mode dispersion in in-line amplifier systems," *Electron. Lett.*, vol. 30, pp. 348–349, Feb. 17, 1994.

[2] M. Yoshimura, T. Kudo, and T. Ozeki, "Polarization mode dispersion equalization," in *Proc. OEC '94*, Makuhari Messe, Japan, 1994, 14E-12, pp. 258–259.

[3] R. Noé *et al.*, "Polarization mode dispersion compensation at 10, 20 and 40 Gb/s with various optical equalizers," *J. Lightwave Technol.*, vol. 17, pp. 1602–1616, Sept. 1999.

[4] H. Rosenfeldt *et al.*, "Automatic PMD compensation at 40 Gbit/s and 80 Gbit/s using a 3-dimensional DOP evaluation for feedback," in *Proc. OFC2001*, PD27-1.

[5] A. Chraplyvy *et al.*, "1-Tb/s Transmission experiment," *IEEE Photon. Technol. Lett.*, pp. 1264–1266, Aug. 1996.

[6] S. Hinz *et al.*, "Interference detection enables 2 $\times$ 20Gbit/s RZ polarization division multiplex transmission," *Electron. Lett.*, vol. 37, pp. 511–512, Apr. 12, 2001.

[7] R. Noé, D. Sandel, S. Hinz, M. Yoshida-Dierolf, V. Mirvoda, G. Feise, H. Herrmann, R. Ricken, W. Sohler, F. Wehrmann, C. Glingener, A. Schöpflin, A. Färbert, and G. Fischer, "Integrated optical $LiNbO_3$ distributed polarization mode dispersion equalizer in 20 Gbit/s transmission system," *Electron. Lett.*, vol. 35, pp. 652–654, Apr. 15, 1999.

[8] C. D. Poole and R. E. Wagner, "Phenomenological approach to polarization dispersion in long single-mode fibers," *Electron. Lett.*, vol. 22, pp. 1029–1030, 1986.

[9] B. H. Billings, "A monochromatic depolarizer," *J. Opt. Soc. Amer.*, vol. 41, pp. 966–975, 1951.

[10] R. Noé *et al.*, "Depolarizer based on acoustooptical TE–TM converters for suppression of polarization holeburning in long haul EDFA links," *Electron. Lett.*, vol. 30, pp. 1500–1501, Sept. 1, 1994.

[11] D. A. Smith and R. Noé, "New polarization scrambler using $Ti:LiNbO_3$ rotating waveplate," in *Proc. IGWO*. Santa Fe, NM: OSA, 1988, pp. 111–114.

[12] H.-M. Rein, "Si and SiGe bipolar ICs for 10 to 40 Gb/s optical-fiber TDM links," *Int. J. High Speed Electron. Syst.*, vol. 9, no. 2, 1998.

[13] R. Noé *et al.*, "Endless polarization control systems for coherent optics," *J. Lightwave Technol.*, vol. 6, pp. 1199–1207, July 1988.

R. Noé (M'93), photograph and biography not available at the time of publication.

D. Sandel, photograph and biography not available at the time of publication.

V. Mirvoda, photograph and biography not available at the time of publication.

F. Wüst, photograph and biography not available at the time of publication.

S. Hinz, photograph and biography not available at the time of publication.